remote sensing

MDPI

Article

An Improved Remote Sensing Retrieval Method for Elevated Duct in the South China Sea

Yinhe Cheng [1], Mengling Zha [1], Wenli Qiao [1,*], Hongjian He [1], Shuwen Wang [2], Shengxiang Wang [1], Xiaoran Li [1] and Weiye He [1]

[1] School of Marine Technology and Geomatics, Jiangsu Ocean University, Lianyungang 222005, China; chengyh@jou.edu.cn (Y.C.); 2020210401@jou.edu.cn (M.Z.); 2021220410@jou.edu.cn (H.H.); 2023220222@jou.edu.cn (S.W.); 2022120490@jou.edu.cn (X.L.); 2020120409@jou.edu.cn (W.H.)

[2] Ocean Institute of Northwestern Polytechnical University, Taicang 215400, China; wangshuwen@nwpu.edu.cn

* Correspondence: qiaowl@jou.edu.cn

Abstract: Elevated duct is an atmospheric structure characterized by abnormal refractive index gradients, which can significantly affect the performance of radar, communication, and other systems by capturing a portion of electromagnetic waves. The South China Sea (SCS) is a high-incidence area for elevated duct, so conducting detection and forecasts of the elevated duct in the SCS holds important scientific significance and practical value. This paper attempts to utilize remote sensing techniques for extracting elevated duct information. Based on GPS sounding data, a lapse rate formula (LRF) model and an empirical formula (EF) model for the estimation of the cloud top height of Stratocumulus were obtained, and then remote sensing retrieval methods of elevated duct were established based on the Moderate Resolution Imaging Spectroradiometer (MODIS) remote sensing data. The results of these two models were compared with results from the elevated duct remote sensing retrieval model developed by the United States Naval Postgraduate School. It is shown that the probability of elevated duct events was 79.1% when the presence of Stratocumulus identified using GPS sounding data, and the trapping layer bottom height of elevated duct well with the cloud top height of Stratocumulus, with a correlation coefficient of 0.79, a mean absolute error of 289 m, and a root mean square error of 598 m. Among the different retrieval models applied to MODIS satellite data, the LRF model emerged as the optimal remote sensing retrieval method for elevated duct in the SCS, showing a correlation coefficient of 0.51, a mean absolute error of 447 m, and a root mean square error of 658 m between the trapping layer bottom height and the cloud top height. Consequently, the encouraging validation results demonstrate that the LRF model proposed in this paper offers a novel method for diagnosing and calculating elevated ducts information over large-scale marine areas from remote sensing data.

Keywords: South China Sea; elevated duct; lapse rate formula; retrieval model; remote sensing data

Citation: Cheng, Y.; Zha, M.; Qiao, W.; He, H.; Wang, S.; Wang, S.; Li, X.; He, W. An Improved Remote Sensing Retrieval Method for Elevated Duct in the South China Sea. *Remote Sens.* **2024**, *16*, 2649. https://doi.org/10.3390/rs16142649

Academic Editors: Yonghong Zhang, Xiefei Zhi, Donglian Sun, Jingyu Wang, Wen Huo and Fei Ge

Received: 29 May 2024
Revised: 12 July 2024
Accepted: 17 July 2024
Published: 19 July 2024

1. Introduction

When electromagnetic waves propagate through the atmosphere, they are influenced by atmospheric refraction, which alters their original propagation path. Under specific meteorological conditions, electromagnetic waves can undergo back-and-forth reflections within a certain atmospheric layer, forming atmospheric duct propagation [1,2]. The atmospheric layer where this propagation phenomenon occurs is called atmospheric duct [3]. The marine environment's unique conditions, such as ocean surface evaporation and temperature inversions, make it a fertile ground for the frequent occurrence of the duct. It has become an important component of marine environment information that affects the navigation of ships at sea, enabling beyond-the-horizon detection or causing detection blind zones [4–8]. Undoubtedly, accurate detection and prediction of the ducts is pivotal for enhancing the performance of radar, communication systems, and weaponry [9].

Generally, ducts are divided into three types: surface, elevated, and evaporation ducts, and they can be defined by the vertical gradient of the modified refractivity (M), where the negative gradient region of the modified refractivity indicates the trapping layer [10]. Elevated duct is one of the main types of atmospheric duct and generally occurs in a higher altitude within the atmosphere. In the marine atmospheric environment, the formation of elevated duct is mainly due to sharp decreases in humidity with height, temperature inversions, or both occurring simultaneously [11,12]. Due to the influence of the marine atmospheric boundary layer with inversions or sharp humidity reductions, most of the global sea area is often continuously covered by elevated duct [13,14].

Studies have shown that Stratocumulus is an important indicator of the presence of elevated duct. The temperature inversion phenomenon is usually observed at the top of Stratocumulus, and the decrease in humidity with height in the inversion layer is considered the most likely mechanism leading to the formation of elevated duct [15–17]. Generally, cloud vertical structure analysis based on GPS sounding data relies mainly on cloud water content. Therefore, atmospheric temperature and humidity obtained from sounding profiles can be used to infer the vertical structure of clouds [18,19]. Currently, the following three methods are commonly used to analyze cloud vertical structure: (1) The Temperature–Dewpoint Difference method, proposed by Poore et al. [20], which determines the vertical information of clouds based on temperature–dewpoint difference profiles using sounding and surface data. However, this method lacks continuity in the vertical structure of clouds. (2) The Relative Humidity Threshold method (also known as WR95 method), initially proposed by Wang et al. [21], which determines cloud layers based on relative humidity profiles. Different temperatures correspond to a single relative humidity, overcoming the limitations of the temperature–dewpoint difference method and providing a continuous cloud layer vertical structure. (3) The Second Derivative method, proposed by Chernykh et al. [22], which utilizes the vertical gradient of atmospheric temperature and humidity to identify cloud layers. The CE method first detects cloud layers using second derivatives and further verifies them using the temperature–dewpoint difference method. Three methods mentioned above have their own advantages and disadvantages. Based on existing research [23,24], most researchers concluded that the Relative Humidity Threshold method was more reasonable since cloud formation primarily occurs when relative humidity tends towards saturation.

Detecting elevated duct using satellite weather maps, cloud images, etc., is an economical and convenient remote sensing method. This method involves analyzing the evolving patterns of weather maps, satellite cloud images, and other meteorological systems to detect the refractive conditions in the relevant marine areas and extract characteristic information about atmospheric duct. In the early 1970s, the United States Navy proposed a plan called the "Refraction Impact Guide", aiming to detect atmospheric refraction based on weather features. However, the final results were unsatisfactory. In 1990, studies conducted preliminary explorations on the inversion of elevated duct using weather satellite images [25,26]. In 1994, the refractive structure was associated with weather, mesoscale, and satellite data parameters by the Naval Air Warfare Center Weapons Division. They discovered that trapping layer was closely associated with anticyclones and pointed out that the trend in both cloud and inversion characteristics correlated well with the occurrence, height, and intensity of elevated ducts, as observed from a large number of radio soundings, which were conducted from the eastern and central north Pacific Ocean [27]. By statistically analyzing the profile refractive data from radio soundings on global coasts, islands, and ships, it was also found that the diurnal climate variation of elevated duct is related to the diurnal variation of marine Stratocumulus cover. Based on this theory, the United States Navy proposed the Satellite Marine-layer/Elevated Duct Height (SMDH) technique, which emphasizes the importance of cloud top temperature and sea surface temperature in determining the height of elevated duct on the West Coast of the United States [28,29]. The United States, based on the quantitative relationship between elevated duct and clouds, developed an expert system guide for assessing elevated duct in the northeastern Pacific

using weather maps and satellite cloud images. In 2000, based on 24 datasets, Jordan [30] confirmed and validated the inversion heights of elevated duct using the SMDH technique and the Naval Postgraduate School (NPS) physical model. It was concluded that valid information about elevated duct could be extracted from satellite remote sensing data, and the NPS physical model had advantages over the statistical model.

In China, research on the inversion of elevated duct using satellite cloud images started relatively late. Hao et al. [31] conducted a case study along the Chinese coast using cloud classification and cloud top temperature from FY-2G satellite and analyzed the feasibility of using satellite remote sensing to invert elevated duct. It emphasized that compared to cloud top temperature data from the FY-2G satellite, using the higher-resolution MODIS data can better capture the elevated duct information. Based on GPS sounding and satellite observations, Li et al. [32] summarized the relationship between various types of low clouds and the occurrence of elevated duct in the western Pacific. They found significant differences in observations between islands and oceans, and generally, the heights of elevated duct were lower than the heights of clouds, but a quantitative relationship between duct parameters and various low cloud heights was not provided.

According to the above studies, the satellite remote sensing inversion method for elevated duct is a feasible approach. By utilizing meteorological satellite data to obtain various meteorological information in the presence of Stratocumulus, it is possible to indirectly obtain information about elevated duct. Thus, two new models, including the lapse rate formula (LRF) model and the empirical formula (EF) model, for estimating the cloud top height of Stratocumulus based on ship-based GPS sounding data, are introduced. Furthermore, the accuracy and precision of satellite remote sensing inversion for elevated duct need to be further investigated. Therefore, these models are validated against the established duct remote sensing retrieval models that are applicable to other regions.

Until now, there are few reports on the satellite remote sensing inversion method for elevated duct, and it remains uncertain whether this method is applicable to the South China Sea (SCS), which is a high-incidence area of atmospheric duct due to the unique geographical location and complex air–sea interactions. This paper takes the SCS as the research area and attempts to explore the models of remote sensing inversion for elevated duct based on satellite data. This exploration enhances the capability to detect elevated ducts in the SCS, filling a gap in existing research and providing a foundation for further studies in other high-incidence ocean regions.

2. Data and Methods

2.1. Data

2.1.1. GPS Sounding Data

There are two sources of high-resolution ship-based GPS sounding data, including data from the "Kexue 1" and "Shiyan 3" research vessels collected during the 1998 SCS Monsoon Experiment, as well as data from the NSFC Open Voyage collected between 2006 and 2012. The main sensors used in these measurements are Vaisala and China Changfeng. Detailed data for each cruise can be found in [1]. The observed parameters include altitude, atmospheric temperature, atmospheric pressure, dew point temperature, relative humidity, wind speed, etc. Observations were typically conducted at 00:00, 06:00, 12:00, and 18:00 UTC daily, with a sampling interval along the profiles of either 1 or 2 s.

Since GPS sounding profile data may contain errors or inaccuracies due to various factors, such as weather conditions, human errors, and instrument limitations, therefore, quality control procedures are applied to eliminate unreasonable or erroneous data. The main steps are as follows:

(1) Removal of unrealistic values in the vertical profiles. The measured atmospheric temperature must be within the range of −80 °C to 45 °C.
(2) The atmospheric temperature must be higher than the dew point temperature.
(3) Under normal circumstances, the altitude should increase with time. Therefore, data with decreasing or constant altitude values over time should be removed.

After applying these quality control procedures, a total of 1081 profile data points were obtained, as shown in Table 1. The distribution of observation stations can be seen in Figure 1.

Table 1. Detailed information of the GPS sounding observations.

Observation Sites	Observation Time	Number
Kexue 1	2 May–24 June 1998	151
Shiyan 3	6 May–23 June 1998	149
Marine observations	8–28 September 2006	41
	26 November–16 December 2006	28
	15–23 May 2007	14
	2–20 June 2007	52
	13 August–29 September 2007	43
	16–19 March 2008	14
	29 June–13 July 2008	29
	15 August–4 September 2008	62
	14 June–4 July 2009	31
	1–19 September 2009	55
	14 April–27 May 2010	53
	2–20 September 2010	57
	26 October–11 November 2010	39
	2–6 April 2011	16
	10–13 May 2011	23
	17 June–3 July 2012	30
	9 August–30 September 2012	133
	7–26 October 2012	61
Total		1081

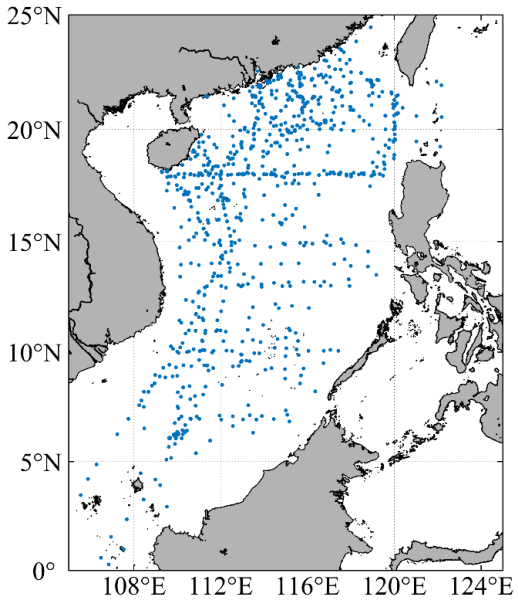

Figure 1. Distribution of GPS sounding stations.

2.1.2. ERA5 Reanalysis Data

ERA5 reanalysis data are the latest generation of the global reanalysis dataset produced by the European Centre for Medium-Range Weather Forecasts (ECMWF), which combine observations with simulated data through data assimilation. This dataset provides global data from January 1940 to the present, including primary data on atmospheric, land, and ocean climate variables. The ERA5 data used in this paper have a spatial resolution of 0.25° × 0.25° for 24 h per day from 1998 to 2012. The data parameters include sea

surface temperature, atmospheric temperature, specific humidity, and others. Since the GPS sounding data are released at least 5 m above the sea surface on the deck of the ship, and the lowest position of GPS detection is susceptible to ship heat contamination, this paper selected the sea surface temperature from ERA5 reanalysis data after bilinear interpolation as the sea surface temperature at the location of the GPS sounding data.

2.1.3. MODIS Data

MODIS sensor is a new generation optical instrument developed by National Aeronautics and Space Administration (NASA). It is carried on two sun-synchronous polar-orbiting satellites, namely, the Terra (morning) and Aqua (afternoon) satellites. These satellites complement each other in updating frequency and provide data with high temporal and spatial resolutions, as well as multispectral capabilities [33]. In this paper, MODIS data were selected as the basic data for the remote sensing inversion of elevated duct. The data are processed by NASA to generate standardized products, including MOD/MYD03 and MOD/MYD06. MOD/MYD03 is a geolocation file containing geographical information for MOD/MYD06 products. MOD/MYD06 is cloud product data, which mainly include cloud top pressure, cloud top height, cloud top temperature, cloud optical thickness, and other cloud parameters, with a spatial resolution of 1 km.

Since the MODIS MOD/MYD06 products only contain information on single-layer clouds and lack cloud type parameters, this paper considers using the cloud classification scheme from the International Satellite Cloud Climatology Project (ISCCP) to classify the MOD/MYD06 products. The ISCCP classifies clouds based on cloud top pressure and cloud optical thickness, as shown in Figure 2.

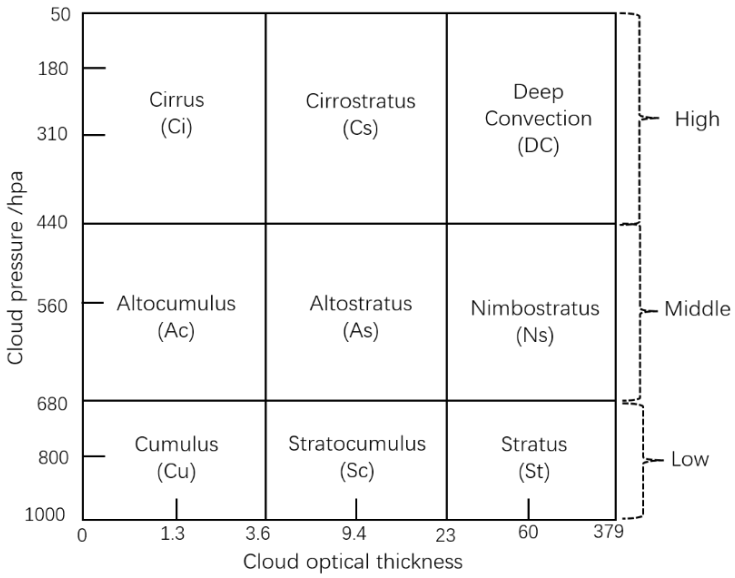

Figure 2. ISCCP cloud classification [34].

According to the ascent time of MODIS, the GPS sounding data from 2006 to 2012 were selected to match it. This is considering that the existing GPS sounding data are launched at four different times: 00:00, 06:00, 12:00, and 18:00 UTC, and the Terra and Aqua satellites carrying MODIS would pass over the China region at around 10:30 a.m. and 1:30 p.m. Beijing time, respectively. Therefore, for the spatiotemporal matching between MODIS and GPS sounding data, the GPS sounding data were used as the reference. MODIS data points within 1 h and within a distance of 0.125° (approximately 13.88 km) from a GPS sounding data were selected. If multiple MODIS data points were matched with individual sounding data, their values were averaged.

2.2. Methodology

2.2.1. Principle of GPS Sounding Data Inversion of Elevated Duct

Duct is usually described using a modified refractivity M (in **M** units) profile. Once the modified refractivity profile is determined, the height of the duct can be calculated. We modelled GPS sounding data using a multi-parameter elevated duct equation, and this equation is adopted from [35], in which the propagation of electromagnetic waves in the atmosphere is corrected by the Earth curvature. The expression for M is as follows:

$$M = 77.6/T(p + 4810e/T) + 0.157h \quad (1)$$

where T denotes the atmosphere temperature in Kelvin (K), p represents the atmospheric pressure in hectopascals (hPa), e denotes the water vapor pressure in hectopascals (hPa), and h represents the altitude in meters (m). All these parameters are available from the GPS sounding profile data. According to the definition of M in Equation (1), the sharp vertical decrease in temperature inversion is conductive to the formation of elevated ducts. The trapping layer is the layer with $dM/dz < 0$, as shown the blue area in Figure 3. This figure illustrates the vertical distribution of the modified refractivity of an ideal elevated duct in relation to temperature and dew point temperature. The upper and lower boundaries are the trapping layer top height and trapping layer bottom height, respectively.

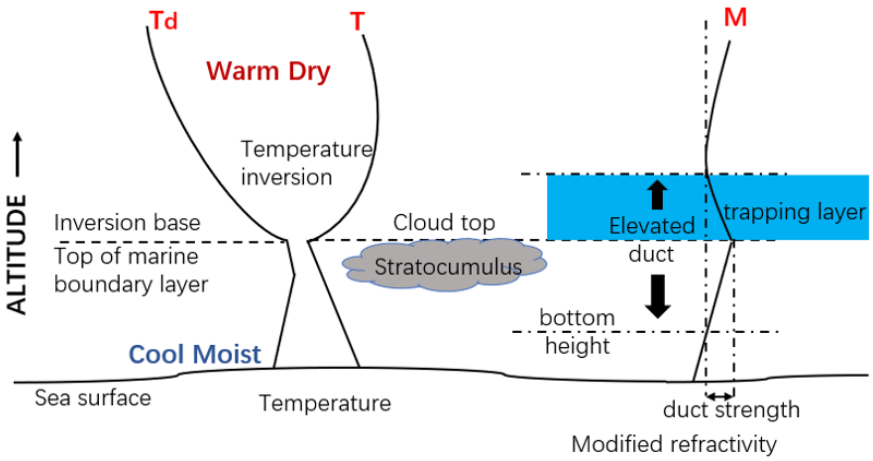

Figure 3. Relationship between atmospheric modified refractivity and air/dew point temperature profiles under an ideal elevated duct condition [17].

2.2.2. Principle of GPS Sounding Data Inversion of Clouds Structure

As mentioned in the introduction, the Relative Humidity Threshold method is a more reasonable method for inverting the vertical structure of clouds. This paper adopts this method to invert the vertical cloud structure using GPS sounding data. The specific determination method is as follows: (1) Determination of Stratocumulus base height (from the bottom to the top of the profile): When the relative humidity (RH) at a certain layer is ≥84%, regardless of whether the humidity is in the near-surface layer or non-near-surface layer, the height of that layer is considered as the base height of the first cloud layer. For the second and subsequent cloud layers, the corresponding height is determined within the humidity layer with RH ≥84%. (2) Determination of Stratocumulus top height (from the top of the profile to the bottom): If the relative humidity (RH) at a certain layer is ≥84%, the height of that humidity layer is considered as the cloud top height. (3) Determination of Stratocumulus layers: If no cloud top height information is found (unless the cloud top height exceeds the top of the profile) or the maximum relative humidity of the cloud layer is <87%, the humidity layer should not be considered as a cloud layer.

According to the research, the Stratocumulus base height in the SCS is below 2.5 km, and the cloud top height ranges from 0.5 to 4.5 km. Therefore, this paper incorporated relevant theories of the marine atmospheric boundary layer and the spatial resolution of

GPS sounding profiles in the SCS to add the following restraint conditions for determining Stratocumulus cloud top height: (1) The cloud base height is less than 2.5 km. If the base height of a cloud layer is greater than 2.5 km, it is discarded. (2) The cloud top height is between 0.5 and 4.5 km. If the top height of a cloud layer is less than 0.5 km, it is discarded. (3) If the top height of a cloud layer is greater than 4.5 km and the cloud base height is less than 2.5 km, the cloud top height is considered as 4.5 km.

2.2.3. Establishment of Remote Sensing Inversion Models

As illustrated the Figure 3, it can be observed that there is a good correspondence between the trapping layer bottom height of the elevated duct and the cloud top height of Stratocumulus over the ocean, providing a better theoretical basis for the satellite remote sensing inversion of elevated duct. In terms of horizontal distribution, the coverage range of Stratocumulus is the same as the range of elevated duct, and the movement, generation, or disappearance of Stratocumulus can reflect the variations in elevated duct. Additionally, in the vertical domain, the inversion and sharp decrease in humidity at the top of Stratocumulus are also the main causes of duct formation, establishing a close relationship between Stratocumulus and elevated duct in three-dimensional space. Therefore, by utilizing meteorological information during the presence of Stratocumulus obtained from GPS sounding profile meteorological data, it is possible to indirectly retrieve the elevated duct.

The U.S. Navy has pointed out that cloud top temperature and sea surface temperature are important factors for determining the height of the elevated duct, which is commonly observed on the west coast of the United States. Research conducted by the Naval Postgraduate School in California has validated the applicability of the SMDH technique and the NPS physical model for this region. In the following work, these two inversion models are also selected to validate the application over the SCS region; further, two inversion models are developed based on the GPS sounding data as we mentioned in Section 2.1.1. Four models are introduced as below:

(1) SMDH technique

The SMDH empirical relation between cloud top height and temperature difference was derived using a best-fit curve based on research cruise data from the eastern Pacific from 1949 to 1952. It should be emphasized that data did not include sea surface temperature, so monthly sea-surface temperature climatology was used [30]. The relationship is as follows:

$$\Delta T = T_{CloudTop} - T_{SeaSurface} \quad (2)$$

$$Z_{CloudTop} = -75.43 \times \Delta T + 2.105 \times (\Delta T)^2 \quad (3)$$

where ΔT represents the temperature difference between the cloud top and the sea surface, measured in degrees Celsius (°C), and $Z_{CloudTop}$ represents the cloud top height in meters (m). This method can only be used when $\Delta T < 0$. If $\Delta T > 0$, a scalar value of 50–100 m will be empirically assigned for the cloud top height.

(2) NPS physical model

NPS physical model estimates cloud top height based on estimates of cloud-base height and vertical cloud fraction (percent), as shown in Figure 4. In a well-mixed marine Stratocumulus boundary layer, if the temperature difference between the cloud-top temperature ($T_{CloudTop}$) and sea-surface temperature ($T_{SeaSurface}$) is small, the observed temperature difference (ΔT) between cloud top and sea surface, along with the cloud top height ($Z_{CloudTop}$), can be used to estimate the total boundary layer lapse rate, $\Gamma = \Delta T / Z_{CloudTop}$. In a well-mixed boundary layer without clouds, the temperature difference divided by the boundary layer depth approximates the dry adiabatic lapse rate. If the cloud layer covers the entire depth of the boundary layer, the lapse rate approximately equal to the moist adiabatic lapse rate. In most marine Stratocumulus boundary layers, the cloud does not fill the entire depth, and there is non-cloudy air beneath the cloud layer. Therefore, it is expected that the observed lapse rate falls between the dry and moist adiabatic lapse

rates. The specific steps of the NPS model are described in the research conducted by Jordan et al. [30].

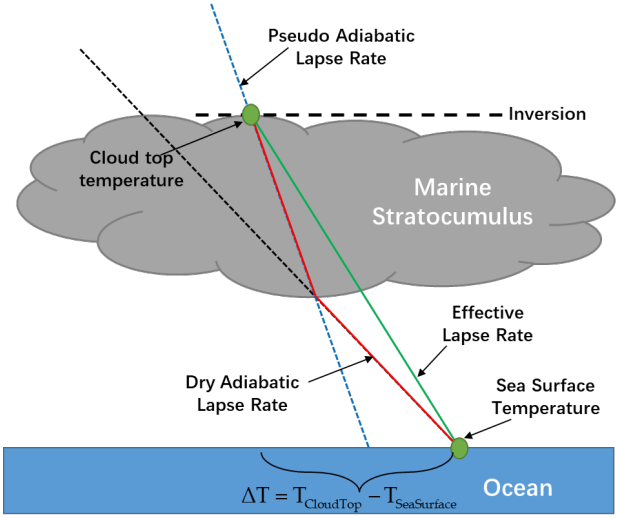

Figure 4. The NPS physical model. The green line shows the effective lapse rate, and the red line shows the dry adiabatic lapse rate (for cloud-free region) and pseudo-adiabatic lapse rate (for cloud region) [30].

(3) Empirical Formula (EF) model

Inspired by the formula of SMDH technology, an empirical formula fitting between the cloud top height and temperature difference based on GPS sounding data over the SCS is proposed. The formula is as follows:

$$Z_{CloudTop} = 2.11 \times (\Delta T)^2 - 125.16 \times \Delta T - 0.11 \quad (4)$$

where ΔT represents the temperature difference between the cloud top height and the sea surface, measured in degrees Celsius (°C), and $Z_{CloudTop}$ represents the cloud top height in meters (m). If the calculated cloud top height is less than 0, it is considered as 0. EF (short for empirical formula) is introduced for conveniently describing the empirical formula model.

(4) Lapse Rate Formula (LRF) model

Utilizing the sea surface temperature, cloud top height, and cloud top temperature from the GPS sounding data over the SCS, the effective lapse rate (Γ) is estimated and the value is -7.1 °C/km. According to the expression form of the NPS physical model, this value is substituted into the following formula to solve for the cloud top height.

$$Z_{CloudTop} = \left(T_{CloudTop} - T_{SeaSurface}\right)/\Gamma \quad (5)$$

where $T_{SeaSurface}$ represents the sea surface temperature in degrees Celsius (°C), $T_{CloudTop}$ represents the cloud top temperature in degrees Celsius (°C), and $Z_{CloudTop}$ represents the cloud top height in meters (m). In the same way, LRF (short for lapse rate formula) is introduced for conveniently describing the lapse rate formula model.

3. Validation and Analysis

3.1. Evaluation Indicators

This paper evaluated the relationship between the elevated duct and Stratocumulus using Pearson correlation coefficient, mean absolute error, and root mean square error. Pearson correlation coefficient (R) measures the degree of correlation between the parameter x and y, and is calculated as follows:

$$R = \frac{\sum_{i=1}^{n}(x_i - \overline{x})(y_i - \overline{y})}{\sqrt{\sum_{i=1}^{n}(x_i - \overline{x})^2}\sqrt{\sum_{i=1}^{n}(y_i - \overline{y})^2}} \quad (6)$$

Mean absolute error (MAE) represents the magnitude of errors of the parameter y with respect to parameter x, and it is calculated using the following formula:

$$MAE = \frac{\sum_{i=1}^{n}|x_i - y_i|}{n} \quad (7)$$

Root mean square error (RMSE) represents the deviation between the parameter x and y. It is calculated using the following formula:

$$RMSE = \sqrt{\frac{\sum_{i=1}^{n}(x_i - y_i)^2}{n}} \quad (8)$$

Specifically in this paper, x represents the detected values based on the GPS sounding data, which represents the value of the cloud top height of Stratocumulus or the trapping layer bottom height. y represents the detected values or the inversion values of the cloud top height of Stratocumulus. n represents the sample size, and i represents the i-th sample. $\overline{x}$, $\overline{y}$ represents the average value of x and y, respectively.

3.2. Statistical Analysis for Detected Stratocumulus and Elevated Duct

Based on the methods for determining Stratocumulus cloud height and the elevated duct using GPS sounding data, statistical analysis was performed, as shown in Table 2.

Table 2. Statistical table for elevated duct and Stratocumulus.

GPS Sounding Data	Elevated Duct (Present)	Elevated Duct (Absent)	Total
Stratocumulus (present)	336	89	425
Stratocumulus (absent)	454	202	656
Total	790	291	1081

As shown in Table 2, the probability of duct occurrence in the GPS sounding data was 73% (790 out of 1081 observations), with 425 occurrences of Stratocumulus identified. The probability of Stratocumulus cloud occurrence was 39.3% (425/1081), and among these, the percentage of Stratocumulus associated with duct events was 79.1% (336/425). This can effectively demonstrate that there was a high probability of duct events occurring in the presence of Stratocumulus.

Based on the results from Table 2, an analysis was conducted on the GPS sounding data that exhibited both duct events and the presence of Stratocumulus. The comparison only focused on the relationship between the duct and the top height of Stratocumulus, considering that the height of the Stratocumulus from MODIS satellite data using in the following work represents the highest height of the Stratocumulus. The results are shown in Figure 5. As shown in this figure, the scatters were well distributed, and the dispersion was relatively limited. The R of the trapping layer bottom height of elevated duct and the cloud top height of Stratocumulus was 0.79, and MAE and RMSE were 289 m and 598 m, respectively.

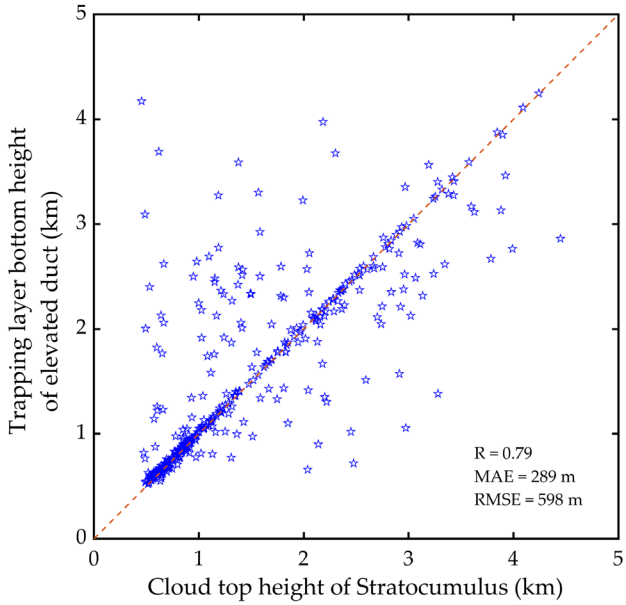

Figure 5. Correlation between cloud top height of Stratocumulus and trapping bottom height of elevated duct.

By randomly selecting a data point that is located on the 1:1 line, an analysis and comparison were conducted between the relative humidity profile indicating the presence of Stratocumulus and the modified atmospheric refractivity profile indicating ducted waves, as shown in Figure 6. It represents the vertical profiles of relative humidity and modified atmospheric refractivity at 6:00 on 16 June 1998. It can be observed that the cloud top height (the green line) was slightly higher than the trapping layer bottom height (the gray line), but both were around 600 m. This indicates a strong correlation between the trapping layer bottom height and the cloud top height of Stratocumulus, which is consistent with the fundamental theory proposed by Helvey et al. [17] regarding duct remote sensing inversion.

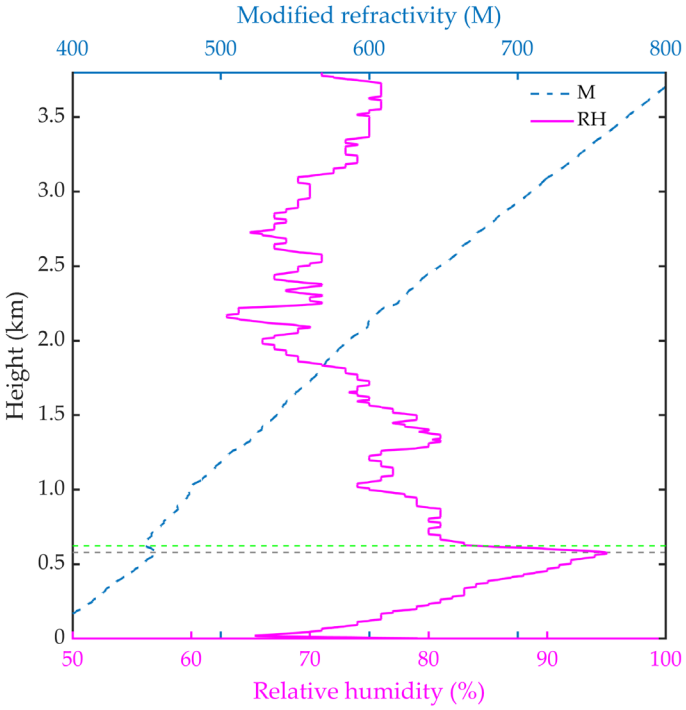

Figure 6. Profiles of relative humidity and atmospheric modified refractivity (the cloud top height was 623 m (green line), and the trapping layer bottom height was 579 m (gray color)).

3.3. Validation of the Remote Sensing Inversion Models

Comparisons between the cloud top heights calculated using the four inversion methods described in Section 2.2.3 and the measured actual cloud top heights and trap bottom heights are also presented in Tables 3 and 4.

Table 3. Correlation between inversion models and measured cloud top heights.

	MAE (m)	RMSE (m)	R
Measured cloud top height	0	0	1
SMDH technique	503	612	0.96
NPS physical model	886	1050	0.94
Empirical formula (EF) model	195	248	0.96
Lapse rate formula (LRF) model	237	316	0.96

Table 4. Correlation between inversion models and measured trapping layer bottom heights.

	MAE (m)	RMSE (m)	R
Measured trapping layer bottom height	0	0	1
Measured cloud top height	289	598	0.79
SMDH technique	545	732	0.74
NPS physical model	819	1045	0.73
Empirical formula (EF) model	407	640	0.75
Lapse rate formula (LRF) model	416	601	0.75

From Table 3, it can be observed that all four inversion methods showed good correlation with the measured cloud top heights in terms of correlation coefficients. In terms of MAE and RMSE, the EF model exhibited the smallest error, with a MAE of 195 m and a RMSE of 248 m. The next best method was the LRF model, with a MAE of 237 m and a RMSE of 316 m. The SMDH technique and NPS physical model followed, with the SMDH technique showing larger errors compared to EF and LRF methods but still within an acceptable range. The NPS physical model, on the other hand, exhibited a RMSE of approximately 1000 m in cloud top height calculations.

As can be seen from Table 4, it can be observed that all four inversion methods showed good correlation with the measured trapping layer bottom height in terms of correlation coefficients. The row "Measured cloud top height" in Table 4 represents the correlation between the measured cloud top heights and trapping layer bottom height, with a correlation coefficient of 0.79, a MAE of 289 m, and a RMSE of 598 m. The correlation coefficients R of the EF model and the LRF model fitted to the SCS were both 0.75, which were only 0.04 lower than the R with measured cloud top height. In terms of MAE, the EF model showed an error that was approximately 100 m higher than the measured cloud top heights, while the LRF model showed a bigger error than the result compared with the EF model. However, the SMDH technique and NPS physical model exhibited higher errors in both MAE and RMSE, especially the NPS physical model, which showed a MAE of 819 m and a RMSE of 1045 m.

Taking into consideration both Tables 3 and 4, it can be concluded that the optimal model was the EF model, followed by the LRF model, with the SMDH technique ranking third, and the NPS physical model performing the poorest.

Since the temperature difference between the atmospheric temperature and sea surface temperature is a common factor associated with the above four inversion methods, the relationship between the inversion methods and the measured data can be visualized by plotting the temperature difference versus the cloud top height, as shown in Figure 7.

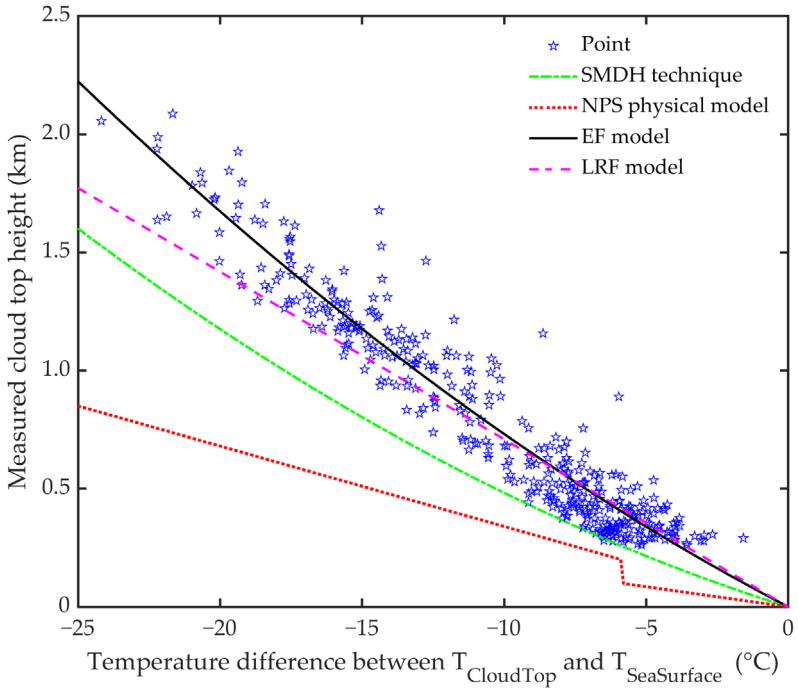

Figure 7. Relationship between cloud top height and temperature difference between the cloud top and the sea surface.

As can be seen from Figure 7, the higher the temperature difference, the higher the cloud top height. Due to the limitation of Stratocumulus height, the cloud top height was mainly concentrated within 0.5~3 km. From the figure, it can be seen that within this height range, the temperature difference generally fell between −15 °C and −5 °C. The figure also includes linear plots for the four inversion methods, and it can be observed that the EF model (black) showed the best correlation with the measured data, primarily concentrated on both sides of the line. The LRF model (magenta) followed, where it tended to overestimate cloud top heights at lower temperatures and heights, while underestimating cloud top heights at higher temperatures and heights. The turning point for the temperature difference was approximately −15 °C. The SMDH technique (green) consistently underestimated the Stratocumulus cloud top heights over the SCS. According to the SMDH technique description, it is only applicable within the range of −15 °C to 0 °C. It was also found that within this range, although the SMDH technique underestimated the cloud top height over the SCS, the underestimation was relatively small, not exceeding 1000 m. Additionally, as the temperature difference decreased, the underestimation also decreased. However, when the temperature difference was less than −15 °C, the underestimation gradually became larger. The NPS physical model (red) performed the poorest among the four methods, consistently underestimating the Stratocumulus cloud top height over the SCS. Moreover, as the temperature difference increased, the underestimation became progressively larger.

4. Application and Comparative Analysis of Remote Sensing Inversion Models

There was a good correlation between the trapping layer bottom height of elevated duct and the cloud top height of Stratocumulus, so the way in which to obtain the relevant information of clouds became the key for inversing elevated duct. Currently, satellite remote sensing technology plays an increasingly important role in cloud detection due to its wide observation range and long duration. In this section, the accuracy of the four inversion models is evaluated using MODIS satellite remote sensing data.

There were 74 matched points after matching MODIS Stratocumulus data with sounding data, and the probability of elevated duct occurrence was 91.9% (68/74). The data

points that corresponded to both duct events and Stratocumulus were picked for the following analysis. Due to the fact that MODIS data only had cloud top height products, the relationship between MODIS Stratocumulus cloud top height products and elevated duct trapping layer bottom height is discussed firstly, as shown in Figure 8.

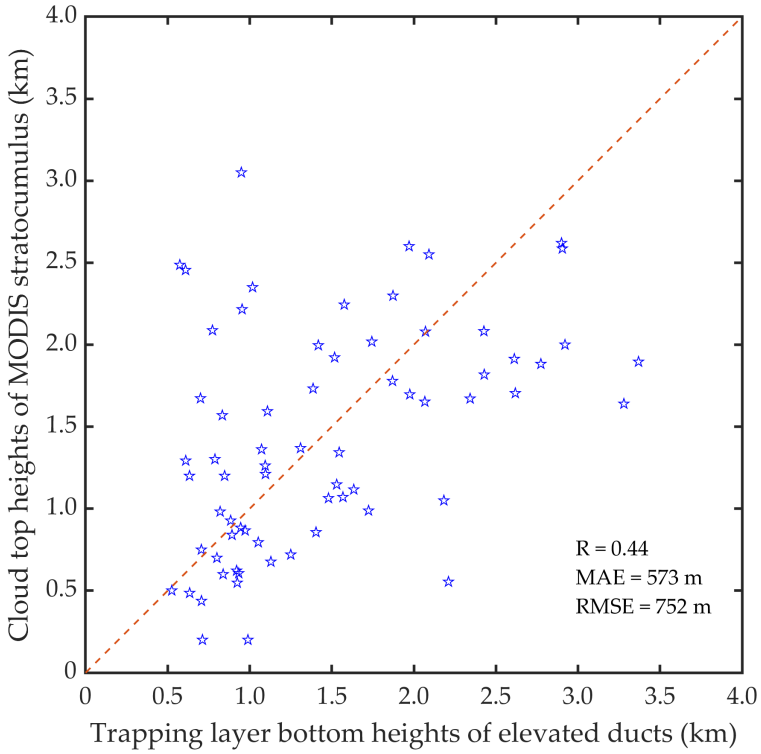

Figure 8. Relationship between trapping layer bottom height and cloud top height of MODIS Stratocumulus.

From Figure 8, it can be observed that although the points were distributed on both sides of the 1:1 line, their distribution range was relatively scattered. When both cloud top height and trapping layer bottom height were below 1 km, the cloud top height was slightly lower than the trapping bottom height, and the data points were mostly close to the 1:1 line. However, when the height exceeded 1 km, the error between them increased. Moreover, as the height increased, the data points became more diffuse, resulting in larger errors. This led to a moderate correlation between the trapping layer bottom height of elevated duct and the cloud top height of MODIS products, with a correlation coefficient of 0.44, a MAE of 573 m, and a RMSE of 752 m.

Figure 9 illustrates the relationship between MODIS Stratocumulus cloud top height calculated using the four inversion models and the trapping layer bottom height of elevated duct. From Figure 9a, it can be observed that when both cloud top height and trapping layer bottom height were below 1000 m, although the cloud top height was slightly lower, the two heights were generally consistent, indicating a good correlation. However, when the height exceeded 1000 m, the cloud top height calculated by the SMDH technique was significantly underestimated, and the discrepancy between the two increased with the trapping layer bottom height of the elevated duct. Figure 9b shows that the cloud top height calculated by the NPS model had a poor correlation with the trapping layer bottom height of the elevated duct. Overall, the cloud top height was consistently lower than the trapping layer bottom height, and since the NPS calculation typically does not exceed 1000 m, the discrepancy between the two increased with higher trapping layer bottom height. Figure 9c depicts the relationship based on the EF model, and it can be observed that the data points were distributed on both sides of the 1:1 line. Figure 9d represents the relationship using a lapse rate of −7.1 °C/km between the cloud top height and the

trapping layer bottom height. The data points were also distributed on both sides of the 1:1 line, similar to Figure 9c. When the height was below 2000 m, the cloud top height calculated by the LRF model was slightly higher than the trapping layer bottom height, while it was lower for height above 2000 m. From this subfigure, it can be noted that the cloud top height calculated by the EF model was slightly higher than that calculated by the LRF model.

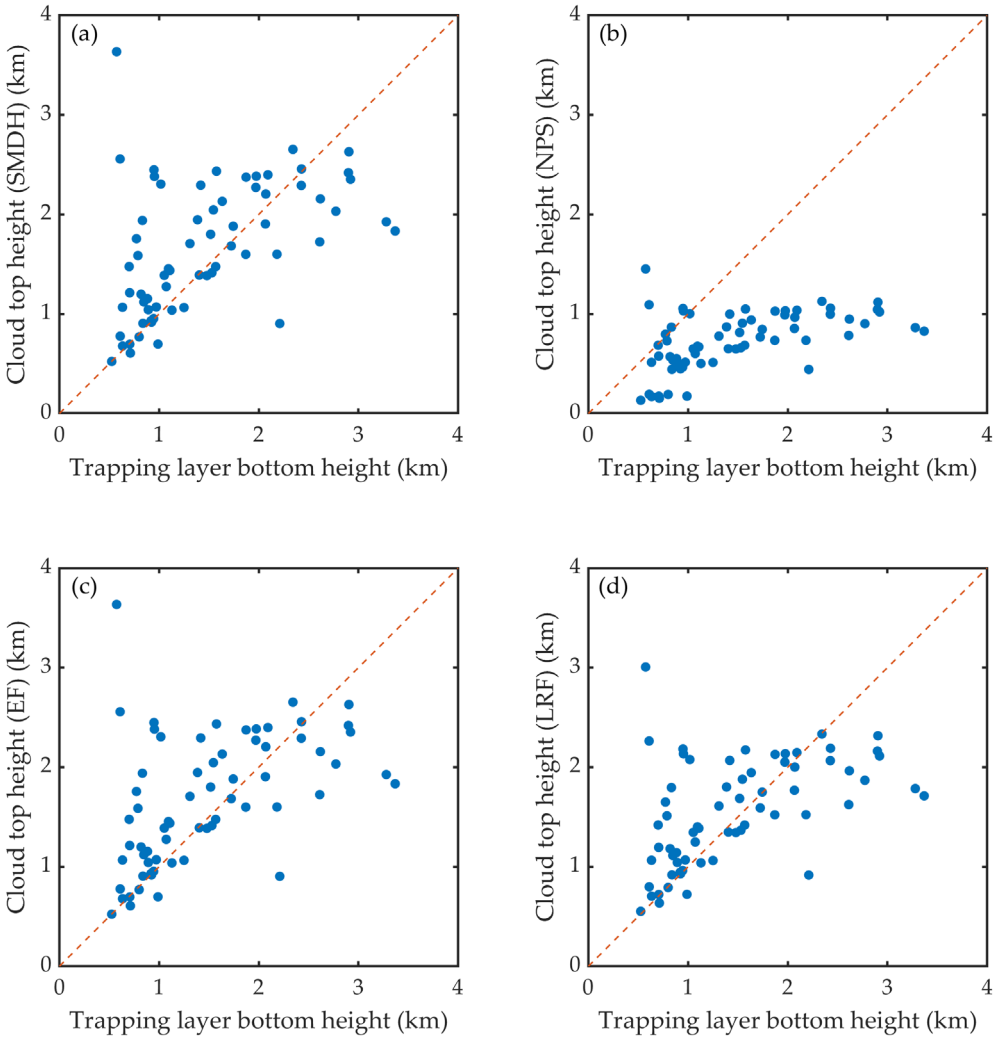

Figure 9. Relationship between trapping bottom height of elevated duct and cloud top height of Stratocumulus calculated by four inversion methods. (**a**) SMDH; (**b**) NPS; (**c**) EF; and (**d**) LRF.

In order to accurately describe the relationship between the cloud top height of MODIS Stratocumulus calculated by different inversion models and the trapping layer bottom height of elevated duct, comparative analysis was conducted using evaluation metrics, as shown in Table 5.

According to Table 5, in terms of correlation coefficients, the four inversion models showed higher correlation with the trapping bottom height of the elevated duct compared to the cloud top height of MODIS products. Among them, the NPS physical model performed the best. Considering the MAE and RMSE, the LRF model yielded the best results, with the smallest MAE of 447 m and RMSE of 658 m. The EF model followed, with error values of 483 m and 726 m. The SMDH technique and MODIS products had larger errors, while the NPS physical model exhibited the largest errors. Overall, among these four inversion methods, the LRF model performed the best, followed by the EF model and the SMDH technique, with the NPS physical model being the least accurate.

Table 5. Correlation between cloud top height of Stratocumulus and trapping layer bottom height of elevated duct.

	MAE (m)	RMSE (m)	R
Measured trapping layer bottom height	0	0	1
cloud top height (MODIS)	573	752	0.44
SMDH technique	554	741	0.49
NPS physical model	777	971	0.52
Empirical formula (EF) model	483	726	0.49
Lapse rate formula (LRF) model	447	658	0.51

5. Application of the Optimal Model

Previous studies have indicated that the outbreak of the summer monsoon in the SCS has a significant impact on the occurrences of elevated duct. In this section, the LRF model is applied to MODIS data to compare and analyze the elevated duct and Stratocumulus that occurred in the SCS during the period of 27–28 June 2012, corresponding to the summer monsoon period. Figure 10 illustrates the distribution of the trapping layer bottom height of the elevated duct and cloud top height of Stratocumulus over the SCS during the coexistence of ducts and clouds from 27 to 28 June.

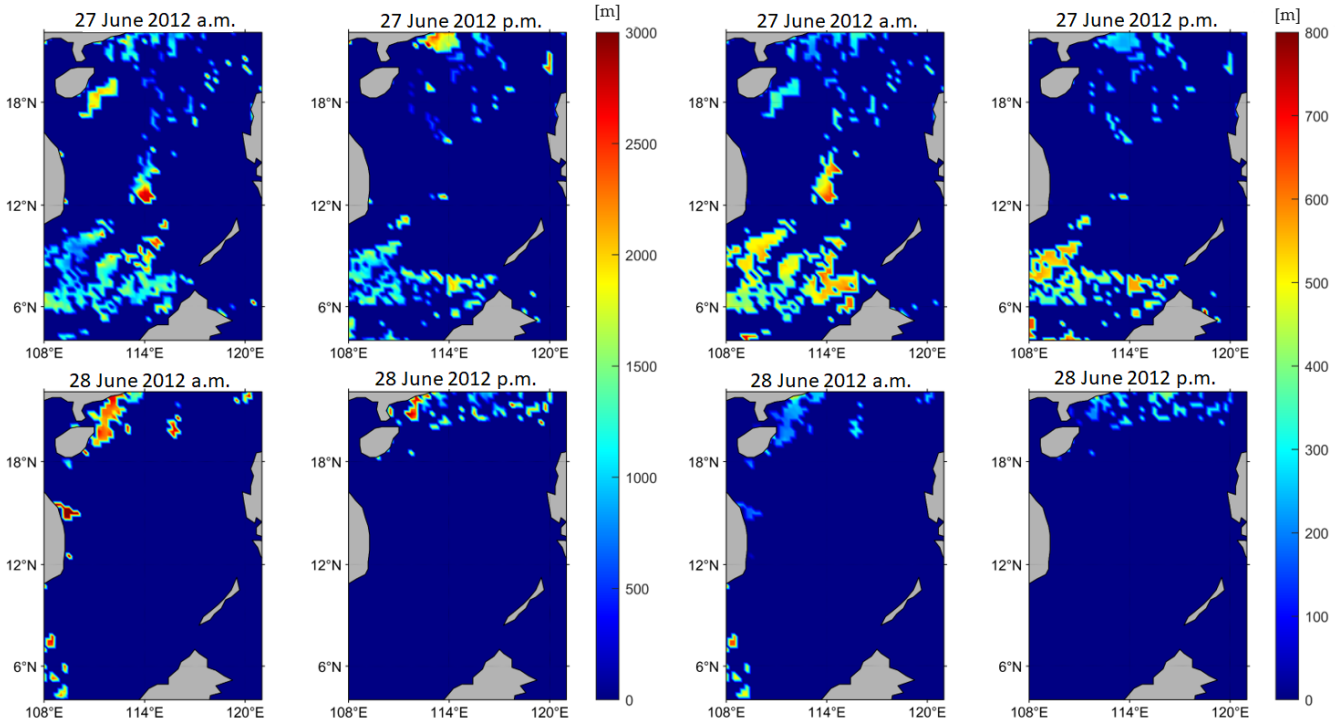

Figure 10. Distribution of the cloud top height of MODIS Stratocumulus (**left panel**) and the trapping layer bottom height (**right panel**) over the SCS on 27–28 June 2012.

From the left panel of Figure 10, it can be observed that on the morning of 27 June, the cloud top height of Stratocumulus in the northern part of the SCS showed a north-to-south decreasing trend. The cloud top height in the northern part was around 1000 m, while the value on the southeast side of Hainan Island was relatively higher, at around 1700 m. The highest cloud top height occurred in the central part of the SCS, at around 2500 m. In the southern part, the cloud top height showed an east-to-west decreasing trend, with height around 1000 m on the western side and around 1500 m on the eastern side. In the afternoon of 27 June, the cloud top height in the northern part of the SCS, particularly near the Leizhou Peninsula, increased to around 1700 m, while the trend in the southern part remained similar to the morning, being slightly higher than the cloud top height. As time

went on, on the morning of 28 June, except for a small cover friction of Stratocumulus along the western and southwestern coasts, the eastern side of Hainan Island experienced a larger presence of Stratocumulus, with cloud top height higher than those on 27 June, at approximately 2500 m. In the afternoon of 28 June, only a few Stratocumuli were present in the northern part of the SCS, with cloud top height of most areas around 1000 m. The cloud top height was higher along the northwest coast, reaching around 2500 m.

As indicated in the right panel of Figure 10, the distribution of the trapping layer bottom height of elevated duct showed a south-to-north decreasing trend on the morning of 27 June. The value in the northern part of the SCS was approximately 300 m, and in the central part it reached its highest state in the morning, up to 700 m. In the southern part, the trapping layer bottom height exhibited an east-to-west decreasing trend, with the values around 500 m and 600 m for the western coastal and the eastern coastal area, respectively. In the afternoon of 27 June, the occurrence of elevated ducts decreased, and there was no significant change in the trapping layer bottom height of the northern area. Also, the trapping layer bottom height in the southern part followed the same trend as the morning, but the cloud top height increased to around 600 m. On 28 June, only a few areas over the SCS presented the elevated duct, with a base height of 200 m in the morning, which rose to around 300 m in the afternoon.

By comparing Figure 10, it can be concluded that the distribution trends of the trapping layer bottom height of elevated duct (Figure 10, right) and the cloud top height of Stratocumulus (Figure 10, left) in the SCS were generally consistent. However, there were significant differences in numerical magnitude along the northern coastal region over the SCS. Overall, the cloud top heights calculated using the LRF model were generally overestimated. The result can be attributed to the fact that the atmospheric temperature in the northern coastal region of the SCS was consistently higher than in the southern part, resulting in higher sea–air temperature differences in the northern part. In addition, the ability of MODIS to retrieve very low clouds (such as Stratocumulus) is limited [36].

6. Conclusions

In this paper, the relationship between elevated ducts and Stratocumulus was verified and analyzed by using ship-based GPS sounding data over the SCS area. Referring to the SMDH (Satellite Marine Layer/Ducting Height) technique and NPS physical model, another two remote sensing inversion models, EF (empirical formula) model and LRF (lapse rate formula), for elevated duct were developed using GPS sounding meteorological data. Furthermore, the four inversion models were applied to invert the elevated duct and were validated using MODIS satellite data. The main conclusions drawn from this paper are as follows:

(1) Based on the GPS sounding data from the SCS, the vertical structure of cloud and the elevated duct were counted. The results show that the probability of identifying duct occurrence associated with Stratocumulus was 79.1%. Moreover, by comparing the relationship between the trapping layer bottom height of elevated duct and the cloud top height of Stratocumulus, a correlation coefficient of 0.79 was found, with a MAE of 289 m and a RMSE of 598 m.

(2) Four models were used for elevated duct inversion. The error analysis was conducted by comparing the cloud top height calculated by the four inversion models with the trapping layer bottom height calculated by the GPS sounding data. The results show that the EF model performed the best among the four inversion models, with a correlation coefficient of 0.75, a MAE of 407 m, and a RMSE of 640 m. The LRF model was the next best, followed by the SMDH technique, while the NPS physical model performed the worst.

(3) Based on MODIS satellite data, the four inversion models were compared and analyzed in the application of satellite remote sensing. The error analysis was conducted by comparing the MODIS cloud top height calculated by the inversion models with the trapping layer bottom height of the elevated duct from GPS sounding data. The

results show that when Stratocumuli were present, the probability of duct occurrence was 91.9%. The LRF model was the optimal remote sensing inversion model, with a correlation coefficient of 0.51, a MAE of 447 m, and a RMSE of 658 m.

(4) The optimal inversion LRF model was selected, and remote sensing applications were conducted over the SCS during the summer monsoon period from 27 to 28 June 2012. The results show that the trapping layer bottom height of the elevated duct was consistently lower than the inverted value of the cloud top height. Synergistic use of AIRS (Atmospheric Infrared Sounder) and MODIS is expected to provide better cloud top height retrievals than from using either one alone [36,37]. However, in terms of the distribution trend and pattern in both of them, there was a good correlation, with a trend of higher heights on the eastern side and lower heights on the western side.

Overall, the LRF model proposed in this paper provides a stirring validation result in inversing the elevated duct based on MODIS satellite data for the SCS area. However, the application of this model in the other types of ducts (such as surface duct), as well as over the other sea areas, is worthy of further research exploration.

Author Contributions: Conceptualization, Y.C.; methodology, M.Z. and W.Q.; validation, M.Z. and H.H.; formal analysis, H.H. and W.H.; investigation, S.W. (Shuwen Wang); data curation, S.W. (Shuwen Wang) and X.L.; writing—original draft preparation, Y.C. and M.Z.; writing—review and editing, W.Q.; visualization, X.L. and S.W. (Shengxiang Wang); supervision, Y.C. and W.Q.; funding acquisition, Y.C. and W.Q. All authors have read and agreed to the published version of the manuscript.

Funding: The work was supported by the National Natural Science Foundation of China (41776029, 62071207, 62341133, 42306036), the China Postdoctoral Science Foundation (2023M731396), the Lianyungang Key Research and Development Program-Social Development (SF2333, SF2232), the Postgraduate Research and Practice Innovation Program of Jiangsu Province (SJCX23-1819) and Practice Innovation Program of Jiangsu Ocean University (KYCX2022-71, KYCX2024-04).

Data Availability Statement: In this study, the MODIS data were downloaded from The Earth Science Data Systems (ESDS) Program (https://search.earthdata.nasa.gov/search, accessed on 29 May 2024), and the ERA5 reanalysis data were from European Centre for Medium-Range Weather Forecasts (ECMWF) Climate Data Store (https://cds.climate.copernicus.eu, accessed on 29 May 2024).

Acknowledgments: The authors thank the Copernicus Climate Change Service for generating and distributing the ERA5 dataset and making them publicly available. We also thank the websites of NASA Earthdata for using MODIS data in this work. Finally, the authors would like to thank the anonymous reviewers for helping to improve the quality of this manuscript.

Conflicts of Interest: The authors declare no conflicts of interest.

References

1. Cheng, Y.; Zhao, Z.; Zhang, Y. Statistical analysis of the lower atmospheric ducts during monsoon period over the South China Sea. *Chin. J. Radio Sci.* **2012**, *27*, 268–274.
2. Guo, X.; Wu, J.; Zhang, J.; Han, J. Deep learning for solving inversion problem of atmospheric refractivity estimation. *Sustain. Cities Soc.* **2018**, *43*, 524–531. [CrossRef]
3. Bean, B.R.; Dutton, E.J. *Radio Meteorology*; National Bureau of Standards Monograph: New York, NY, USA, 1966.
4. Paulus, R.A. *Specification for Environmental Measurements to Assess Radar Sensors*; Naval Ocean Systems Center: San Diego, CA, USA, 1989.
5. Cui, M.; Zhang, Y. Deep learning method for evaporation duct inversion based on GPS signal. *Atmosphere* **2022**, *13*, 2091. [CrossRef]
6. Qiu, Z.; Zhang, C.; Wang, B.; Hu, T.; Li, Z.; Chen, S.; Wu, S. Analysis of the accuracy of using ERA5 reanalysis data for diagnosis of evaporation ducts in the East China Sea. *Front. Mar. Sci.* **2023**, *9*, 1108600. [CrossRef]
7. Sirkova, I. Revisiting enhanced AIS detection range under anomalous propagation conditions. *J. Mar. Sci. Eng.* **2023**, *11*, 1838. [CrossRef]
8. Han, J.; Wu, J.; Zhu, Q.; Wang, H.; Zhou, Y.; Jiang, M.; Zhang, S.; Wang, B. Evaporation duct height nowcasting in China's Yellow Sea based on deep learning. *Remote Sens.* **2021**, *13*, 1577. [CrossRef]
9. Liang, Z.; Ding, J.; Fei, J.; Cheng, X.; Huang, X. Maintenance and sudden change of a strong elevated ducting event associated with high pressure and marine low-level jet. *J. Meteorol. Res.* **2020**, *34*, 1287–1298. [CrossRef]

10. Lim, T.H.; Wang, S.; Chong, Y.J.; Park, Y.B.; Ko, J.; Choo, H. High altitude ducts causing abnormal wave propagation in coastal area of Korea. *Microw. Opt. Technol. Lett.* **2020**, *62*, 643–650. [CrossRef]
11. Haack, T.; Burk, S.D. Summertime marine refractivity conditions along coastal California. *J. Appl. Meteorol.* **2001**, *40*, 673–687. [CrossRef]
12. Liu, S.; Liang, X.Z. Observed diurnal cycle climatology of planetary boundary layer height. *J. Clim.* **2010**, *23*, 5790–5809. [CrossRef]
13. Ding, J.; Fei, J.; Huang, X.; Cheng, X.; Hu, X.; Ji, L. Development and validation of an evaporation duct model. Part I: Model establishment and sensitivity experiments. *J. Meteorol. Res.* **2015**, *29*, 467–481.
14. Zhang, Q.; Yang, K.; Yang, Q. Statistical analysis of the quantified relationship between evaporation duct and oceanic evaporation for unstable conditions. *J. Atmos. Ocean. Technol.* **2017**, *34*, 2489–2497. [CrossRef]
15. Helvey, R.A.; Rosenthal, J.S. *Guide for Inferring Refractive Conditions from Synoptic Parameters*; Technical Report; Pacific Missile Test Center: Ventura County, CA, USA, 1983.
16. Rosenthal, J.S.; Westerman, S.; Helvey, R.A. *Inferring Refractivity Conditions from Satellite Imagery*; Technical Report; Pacific Missile Test Center: Ventura County, CA, USA, 1985.
17. Helvey, R.A.; Rosenthal, J.S.; Eddington, L.; Greiman, P.; Fisk, C. Use of satellite imagery and other indicators to assess variability and climatology of oceanic elevated duct. In Proceedings of the Sensor and Propagation Panel Symposium, Bremerhaven, Germany, 19–22 September 1994.
18. Li, S.; Li, Y.; Sun, G.; Song, W. Cloud microphysical characteristics in the development of stratocumulus over Eastern China. *Chin. J. Geophys.* **2019**, *62*, 4513–4526.
19. Zuidema, P.; Mapes, B. Cloud vertical structure observed from space and ship over the Bay of Bengal and the Eastern Tropical Pacific. *J. Meteor. Soc. Jpn.* **2008**, *86*, 205–218. [CrossRef]
20. Poore, K.D.; Wang, J.; Rossow, W.B. Cloud layer thicknesses from a combination of surface and upper-air observations. *J. Clim.* **1995**, *8*, 550–568. [CrossRef]
21. Wang, J.; Rossow, W.B. Determination of cloud vertical structure from upper-air observations. *J. Appl. Meteorol. Clim.* **1995**, *34*, 2243–2258. [CrossRef]
22. Chernykh, I.V.; Eskridge, R.E. Determination of cloud amount and level from radiosonde soundings. *J. Appl. Meteorol. Clim.* **1996**, *35*, 1362–1369. [CrossRef]
23. Zhou, Y.; Ou, J. The method of cloud vertical structure analysis using rawinsonde observation and its applied research. *Meteor. Mon.* **2010**, *36*, 50–58.
24. Zhang, J.; Chen, H.; Li, Z.; Fan, X.; Peng, L.; Yu, Y.; Cribb, M. Analysis of cloud layer structure in Shouxian, China using RS92 radiosonde aided by 95 GHz cloud radar. *J. Geophys. Res. Atmos.* **2010**, *115*, 1–13. [CrossRef]
25. Rosenthal, J.S.; Helvey, R.A.; Lyons, S.W.; Fox, A.D.; Szymber, R.; Eddington, L. Weather satellite and computer modeling approaches to assessing propagation over marine environments. *Agard* **1989**, *453*, 47.1–47.15.
26. Rosenthal, J.S.; Helvey, R.A. Refractive assessments from satellite observations. *Agard* **1992**, *502*, 8.1–8.9.
27. Richter, J.H. Structure, variability and sensing of the coastal environment. In Proceedings of the Sensor and Propagation Panel Symposium, Bremerhaven, Germany, 19–22 September 1994.
28. Lyons, S.W. *SPADS Automated Duct Height Statistics*; Technical Report; Pacific Missile Test Center: Ventura County, CA, USA, 1985.
29. Helvey, R.A.; Rosenthal, J.S. Guidance for an expert system approach to elevated duct assessment over the Northeastern Pacific Ocean. In Proceedings of the 1994 IEEE International Geoscience and Remote Sensing Symposium, Pasadena, CA, USA, 8–12 August 1994.
30. Jordan, M.S.; Durkee, P.A. *Verification and Validation of the Satellite Marine-Layer/Elevated Duct Height (SMDH) Technique*; Naval Postgraduate School Monterey California Department of Meteorology: Marina, CA, USA, 2000.
31. Hao, X.; Li, Q.; Guo, L.; Guo, X. Preliminary research on inversion method of elevated duct from meteorological satellite observation over Chinese regional seas. *Acta Electron. Sin.* **2019**, *47*, 600–605.
32. Li, X.; Sheng, L.; Wang, W. Elevated duct and low clouds over the Central Western Pacific Ocean in winter based on GPS soundings and satellite observation. *J. Ocean. Univ. China* **2021**, *20*, 244–256. [CrossRef]
33. King, M.D.; Kaufman, Y.J.; Menzel, W.P.; Tanre, D. Remote sensing of cloud, aerosol, and water vapor properties from the Moderate Resolution Imaging Spectrometer (MODIS). *IEEE Trans. Geosci. Remote Sens.* **1992**, *30*, 2–27. [CrossRef]
34. Rossow, W.B.; Schiffer, R.A. Advances in understanding clouds from ISCCP. *Bull. Am. Meteorol. Soc.* **1999**, *80*, 2261–2288. [CrossRef]
35. Zuo, L.; Tu, Y.; Yao, C.; Chen, B. Preliminary Investigation on the Blind of Shipborne OTH Radar Based on Sea Atmospheric Duct. *Fire Control Command Control* **2011**, *36*, 165–168.
36. Weisz, E.; Li, J.; Menzel, W.P.; Heidinger, A.K.; Kahn, B.H.; Liu, C.Y. Comparison of AIRS, MODIS, CloudSat and CALIPSO cloud top height retrievals. *Geophys. Res. Lett.* **2007**, *34*, 1–5. [CrossRef]
37. Li, J.; Zhang, W.; Sun, F.; Schmit, T.J.; Gurka, J.J.; Weisz, E. Synergistic use of MODIS and AIRS in a variational retrieval of cloud parameters. *J. Appl. Meteorol.* **2004**, *43*, 1619–1643. [CrossRef]